Progress In Electromagnetics Research, Vol. 106, 395–417, 2010

ESTIMATION FOR SMALL-SCALE FADING CHARACTERISTICS OF RF WIRELESS LINK UNDER RAILWAY COMMUNICATION ENVIRONMENT USING INTEGRATIVE MODELING TECHNIQUE

S. Pu, J.-H. Wang, and Z. Zhang †

Institute of Lightwave Technology
Beijing Jiaotong University
Beijing 100044, China

Abstract—The small-scale fading behavior in common wireless communication systems can be predicted by a series of propagation models. Although these types of models are feasible and effective for the situations of transmitting/receiving (Tx/Rx) antennas in relatively open surrounding environments, they are unable to address the coupling between the antenna and environment. In order to overcome this difficulty, a full-wave numerical method is applied in terms of the advantage in considering the interaction between complicated environments and the Tx/Rx antennas, and it can take into account the effect of the interaction on signals. In this paper, an integrative modeling technique involving FDTD method, two-path propagation model and multi-path statistical distribution model is presented, which combines the deterministic and statistical methods. For achieving reliable communication especially in high-speed railway environment, high sampling rate and adequate sampling points are needed for analyzing the propagation properties of the radio frequency (RF) link. This can be easily achieved by the integrative modeling technique, and the output voltage and current of train antenna under the illumination of base-station (BS) antenna along the railway can be given in detail. Results obtained from the integrative simulation for three different multi-path statistical distribution models are presented and analyzed.

Received 28 April 2010, Accepted 19 July 2010, Scheduled 28 July 2010
Corresponding author: S. Pu (06111002@bjtu.edu.cn).

† S. Pu, J.-H. Wang, and Z. Zhang are also with Key Laboratory of All Optical Network & Advanced Telecommunication Network, Education Ministry of China, Beijing Jiaotong University, Beijing 100044, China.

1. INTRODUCTION

The reliability of railway communication systems is demanded to be much higher than that of common ones, especially for the cases of high-data-rate and real-time communication between high-speed train and ground. For wireless communications, one of the key factors that affect the quality of the information transmission is the performance of radio frequency (RF) link. It is also the key factor for the railway mobile communication. Therefore, it is very important to study the RF wireless link under the railway environment precisely and to know the characteristics of it clearly. The entire RF wireless link, as we defined in [1], can be divided into three parts: The radiating of RF signal by transmitting (Tx) antenna, the propagating of the wave in space, and the receiving of the RF signal by receiving (Rx) antenna.

Available works are mainly focused on the second part of the RF link as mentioned above. Many theoretical and experimental studies have been carried out to predict the radio propagation characteristics by different kinds of propagation models for land mobile wireless communication environments [2–9]. These studies aim to analyze propagation problems, such as path loss, various fadings, multi-path time-delay spread, etc. Moreover, the physical propagation mechanisms, including line-of-sight (LOS), (multiple) reflections, scatterings and diffractions, are discussed in detail. Basically, most of these works are done for the field-to-field predictions, thus neglecting the interactions between antennas and nearby environment [10–12], or just taking the antenna gain into account [7, 13–15]. In [16, 17], a mean effective gain of antennas is used to evaluate this mutual effect between the antenna gain and propagation characteristics. Therefore, the signal transmission process studied by these conventional methods is actually the space-to-space case, not the terminal-to-terminal case, i.e., the link property is analyzed from one point to another one in space, not from the input terminal of the Tx antenna to the output terminal of the Rx antenna. Of course, these studies are very important and efficient for the design of common wireless communication systems. However, for accurate modeling of the RF wireless link, especially for the case of high-speed railway communication in complicated environment, the interactions between Tx/Rx antennas and their surrounding environments must be taken into account accurately. The influence of the complicated railway communication environment on the receiving and radiating characteristics of antennas is distinct as shown in our previous work [1]. In this paper, an integrative modeling technique, involving full-wave numerical method for precise field-to-circuit calculation and propagation models for field-to-field

prediction, is presented for simulating the entire RF link. Actually, considering the environment effect is not only important for railway communication, but also significant in other aspects. For example, in the design of antenna in the presence of large and complex structures, the interactions are considered to be an important factor and evaluated by different methods or hybridization of commercial softwares [18, 19].

In our previous work [20], an integrative modeling technique combining FDTD method with two-path propagation model was proposed mainly for the large-scale fading characteristics of the RF link effectively, where the RF link is from the base-station (BS) to the train (called RF downlink), and the moving direction of the train is towards the BS. Then the variations of the output signal strength of the train antenna are obtained, while the train is moving over a long-distance of about 3500 m. With the knowledge of wireless channel [21], the large-scale fading is caused by distance-dependent path loss and shadowing effects, which can be considered by the two-path propagation model involved in the integrative modeling technique. However, the small-scale fading is caused by multi-path signals reflected or scattered by the environment obstacles, such as buildings, trees, etc. So the method in [20] is not suitable for this small-scale case. Due to quick fluctuation, the small-scale modeling involves the statistical method. In this paper, a further study on the integrative modeling technique is presented for predicting the small-scale fading characteristics of the RF downlink, which involves not only the FDTD method and two-path propagation model, but also the multi-path statistical distribution model. The method in this paper can be used to evaluate the efficiency of the wireless communication system. This is helpful in designing a wireless communication system with smoother radio wave coverage.

In the following sections, the proposed integrative modeling technique for RF wireless communication system is presented. The simulation results of some small-scale fadings of the RF downlink under high-speed railway environments are given, and three different kinds of multi-path statistical distribution models are considered. The method is verified by comparing the result with that of Ansoft-HFSS. The example used in verification is a receiving monopole mounted upon a conducting rectangular box.

2. THEORY AND METHOD

2.1. Problem Description

The RF wireless downlink considered here is starting from the input terminal of the BS antenna to the output terminal of the antenna on train. It actually is a circuit-to-circuit problem. A typical RF downlink

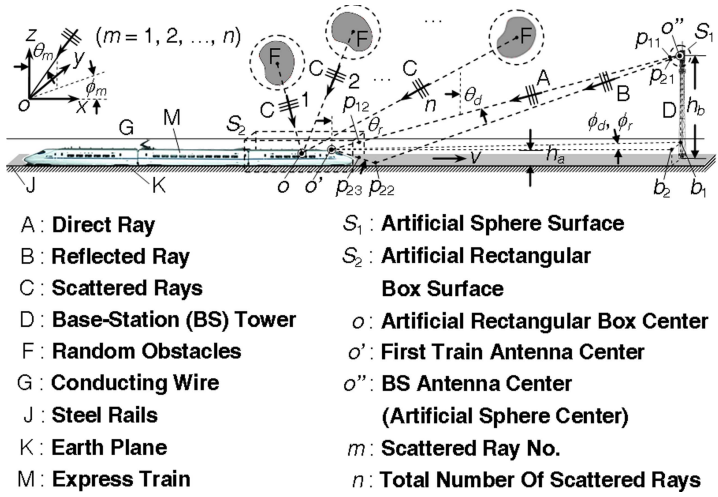

Figure 1. Schematic diagram of RF wireless link downward.

under the railway environment is shown schematically in Fig. 1. The center of the first front antenna mounted on the train locomotive and the center of BS antenna installed on a tower are denoted by points o' and o'' respectively, and their heights are denoted by h_a and h_b. Within the coverage area of BS antenna, the express train is running towards $+x$-direction with velocity of v. In the analysis, two artificial surfaces enclosing link terminals are introduced as shown in Fig. 1: One is a sphere surface centered at o'', which encloses the BS antenna, and is denoted by S_1, while the other is a rectangular box surface centered at o, which encloses the whole train locomotive and its environment, and is denoted by S_2. The two artificial surfaces are the connecting boundaries on which the FDTD method, two-path propagation model and multi-path statistical distribution model are matched. In Fig. 1, o-xyz, o'-$x'y'z'$, and o''-$x''y''z''$ coordinates are parallel with each other.

In the integrative modeling technique, the entire RF downlink is divided into three parts by S_1 and S_2. The link parts containing the near-field regions of Tx/Rx antennas together with surrounding environments within S_1 and S_2 are calculated by the FDTD method, and the far-fields on S_1 are obtained by integrating the equivalent electric and magnetic currents on the output boundary in FDTD computation domain. The Yee's mesh grid [22] and the uni-axial anisotropic PML [23] are used in this paper. The rest part of the link in space from S_1 to S_2 is predicted by the two-path propagation model and the multi-path statistical distribution model. In the calculation, a

voltage source is applied to the feeding terminal of the BS antenna, and the far-fields on S_1 of the BS antenna is obtained. Then the direct and the ground-reflected fields from S_1 to S_2 are traced, and the scattered fields statistically distributed on S_2 are introduced. Finally, the output voltage and current of the train antenna are calculated.

2.2. FDTD Modeling and Analysis Method

2.2.1. Rx Antenna with Surrounding Environment

Considering the limitations of computer memory and running time, the total-field/scattered-field connecting boundary in FDTD computation domain is restricted to S_2, on which the incident waves are introduced. So only the environment near the train antennas is involved, as illustrated in Fig. 1 and Fig. 2. The geometric models used in FDTD include the locomotive body of the express train, train antennas mounted on the locomotive (so-called locomotive antennas), steel rails, earth plane and conducting wire for power supply. In FDTD, the locomotive antennas and their surrounding environment depicted in Fig. 1 are discretized into cubic meshes with grid size of $\Delta S = 0.0333\,\text{m}$, as shown in Fig. 3.

As indicated in Fig. 3, the locomotive has the maximum size of $25.7\,\text{m} \times 3.38\,\text{m} \times 3.63\,\text{m}$ ($771 \times 101 \times 109$ grids correspondingly) and one grid is used to simulate the thickness of it. The windows on both sides of the locomotive are symmetric and made of glass. The conducting wire for power supply has a square cross section of $1\Delta S \times 1\Delta S$ and is located $1.97\,\text{m}$ ($59\Delta S$) above the center of the

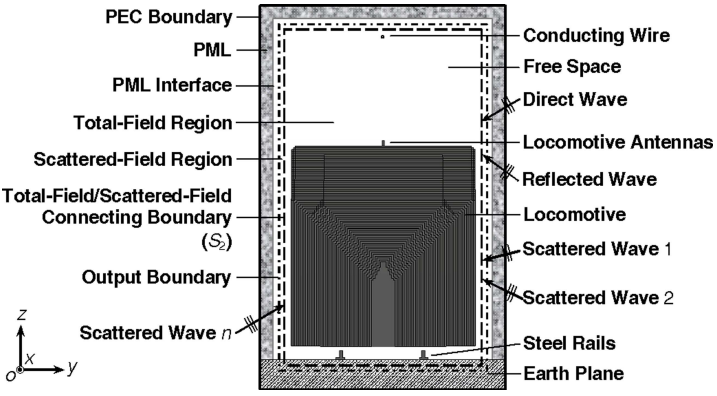

Figure 2. Cross section of FDTD computation domain for modeling Rx antenna and surrounding environment.

locomotive top. The steel rails are located $2\Delta S$ below the bottom of the locomotive with standard gauge of 1.435 m ($43\Delta S$) between them, and the cross sections of the rails are depicted in Fig. 3(d). Other parameters are also given in Fig. 3. In terms of infinity approximation, the objects like the conducting wire, the steel rails and the earth plane below the rails are extended into the PML in FDTD computation, and the electromagnetic material parameters of these objects are listed in Table 1, where μ_r, ε_r and σ denote relative permeability, relative permittivity and electric conductivity respectively.

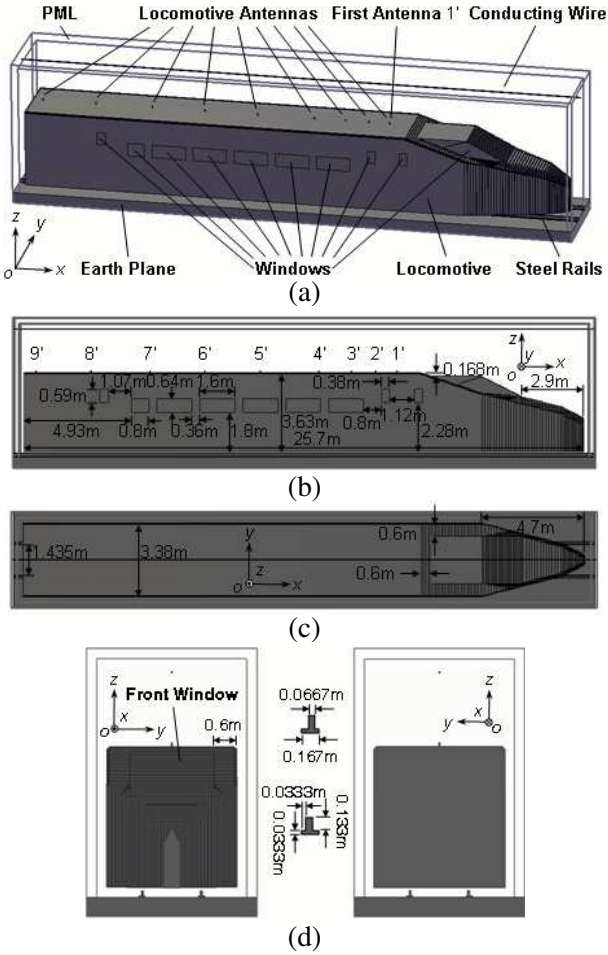

Figure 3. Discretization model of locomotive antennas and their surrounding environment. (a) Three-dimensional view, (b) side view, (c) top view, (d) front and back view.

Table 1. List of the electromagnetic material parameters used.

Object Model	μ_r	ε_r	σ (S/m)
Locomotive Body	1	1	2.494×10^7
Vehicle Windows	1	5.5	0
Conducting Wire for Power Supply	1	1	5.8×10^7
Steel Rails	1	1	1.1×10^6
Earth Plane	1	14	0.01

In this paper, the operating frequency for the Tx/Rx antenna systems is set to 900 MHz. The corresponding wavelength λ is ten times the grid size ($\Delta S = 0.1\lambda$) of FDTD. As shown in Fig. 3, there are total nine monopole antennas (numbered from $1'$ to $9'$) mounted upon the locomotive along the central line. Here, all of them are set to quarter-wavelength monopoles and located at $514\Delta S$, $484\Delta S$, $451\Delta S$, $406\Delta S$, $325\Delta S$, $249\Delta S$, $173\Delta S$, $92\Delta S$ and $16\Delta S$ away from the rear terminal plane of the locomotive respectively. In order to get accurate results, the monopole model proposed in [24] is used, in which the monopole structure as well as the feeding structure by coaxial cable are taken into account. Fig. 4 depicts monopole model of the locomotive antenna $1'$ fed by the coaxial cable with radius a of the inner conductor and radius b of the inner surface of the outer conductor. The others have the same structure but the locations in x'-direction are different. U_{ab} is the voltage of the cable, and I_z is the $+z$-direction current on the inner conductor or the monopole arm (extended from the inner conductor). For the monopole with length of L_1, the thin-wire approximation is made. Different from that in [24], the current $I_z^{n+0.5}(k'+0.5)$ on the arm ($0 \le k' \le 2$) is reformulated as following, which involves four H-field components around the arm cylinder along the integration path of a circle with radius $0.5\Delta S$,

$$\begin{aligned} I_z^{n+0.5}\left(k'+0.5\right) \;=\; & \frac{\pi\Delta x}{4}\left[H_y^{n+0.5}\left(i_a+0.5, j_a, k'+0.5\right)\right. \\ & \left.-H_y^{n+0.5}\left(i_a-0.5, j_a, k'+0.5\right)\right] \\ & -\frac{\pi\Delta y}{4}\left[H_x^{n+0.5}\left(i_a, j_a+0.5, k'+0.5\right)\right. \\ & \left.-H_x^{n+0.5}\left(i_a, j_a-0.5, k'+0.5\right)\right] \end{aligned} \tag{1}$$

where $\Delta x = \Delta y = \Delta S$, and the node (i_a, j_a, k_a) represents the center point o' of the inner conductor at $k' = 0$. For the coaxial line with length of L_2, only a single TEM-mode is used to approximate the fields within it. Then, the coaxial line can be seen as a one-dimension transmission line. Thus, the iterative formulas of the voltage $U_{ab}(k')$

($k'_{\text{foot}} < k' \leq 0$) and the current $I_z(k'+0.5)$ ($k'_{\text{foot}} \leq k' \leq 0$) on the coaxial line can be represented by

$$U_{ab}^{n+1}\left(k'\right) = U_{ab}^{n}\left(k'\right) - \frac{Z_c}{2\sqrt{\varepsilon_{rc}}}\left[I_z^{n+0.5}\left(k'+0.5\right) - I_z^{n+0.5}\left(k'-0.5\right)\right] \quad (2)$$

and

$$I_z^{n+0.5}(k'+0.5) = I_z^{n-0.5}(k'+0.5) - \frac{1}{2Z_c\sqrt{\varepsilon_{rc}}}\left[U_{ab}^{n}(k'+1) - U_{ab}^{n}(k')\right] \quad (3)$$

where ε_{rc} is the relative permittivity of the coaxial dielectric, and the characteristic impedance of the coaxial line is

$$Z_c = \frac{1}{2\pi}\sqrt{\frac{\mu_0}{\varepsilon_0\varepsilon_{rc}}}\ln\left(\frac{b}{a}\right). \quad (4)$$

From (2) and (3), the relationship between the voltage and current on the coaxial line is similar to the iteration formulas of the E-field and H-field in FDTD. For simulating the traveling waves in $-z'$-direction, at the end $k' = k'_{\text{foot}}$ of the coaxial line, Mur's absorbing boundary condition is applied

$$\begin{aligned} U_{ab}^{n+1}\left(k'_{\text{foot}}\right) = {} & U_{ab}^{n}\left(k'_{\text{foot}}+1\right) + \frac{c\Delta t - \sqrt{\varepsilon_{rc}}\Delta z}{c\Delta t + \sqrt{\varepsilon_{rc}}\Delta z} \\ & \times\left[U_{ab}^{n+1}\left(k'_{\text{foot}}+1\right) - U_{ab}^{n}\left(k'_{\text{foot}}\right)\right] \end{aligned} \quad (5)$$

where c is the velocity of light, Δt is the time-step, and the grid size Δz equals to ΔS. In order to synchronize the output voltage and current at integer time-steps $n\Delta t$, the current $I_z^{n+1}(k'+0.5)$ ($k'_{\text{foot}} \leq k' \leq 2$) is given by

$$I_z^{n+1}\left(k'+0.5\right) = \frac{1}{2}\left[I_z^{n+0.5}\left(k'+0.5\right) + I_z^{n+1.5}\left(k'+0.5\right)\right]. \quad (6)$$

2.2.2. Tx Antenna

As shown in Fig. 1, the Tx antenna is the BS antenna which is composed of a four-dipole array (4×1) and a reflector. Unlike the locomotive antennas analyzed above, the environment surrounding the BS antenna is simply the free space. Hence, S_1 only contains the BS antenna itself as shown in Fig. 5. For BS antenna, the size of FDTD meshes is set to $\Delta S' = 0.025\lambda$ for accurately modeling the reflector with narrow edge-folds. The backplane of the reflector is a rectangular copper sheet with size of $0.8\lambda \times 3.75\lambda$, and the two edges folded over 90° are the rectangular copper sheets with size of $0.05\lambda \times 3.75\lambda$. There are four half-wavelength (0.5λ) dipole elements numbered from $1''$ to $4''$ placed along z''-direction about 0.25λ away

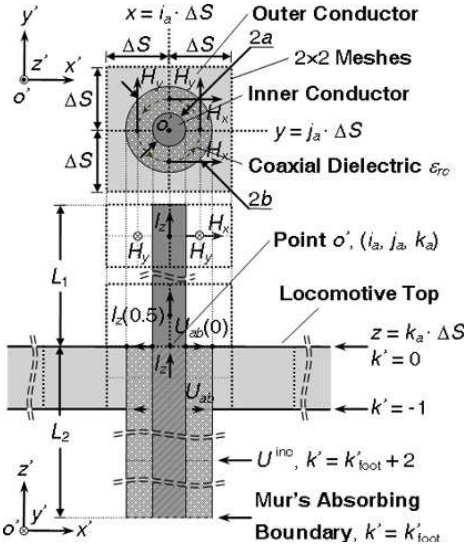

Figure 4. Coax-fed monopole model of antenna $1'$ mounted on locomotive top.

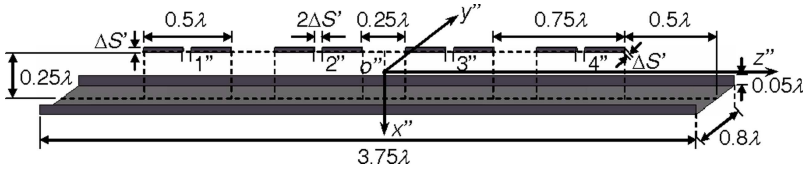

Figure 5. Three-dimensional geometric model of Tx antenna discretized in new FDTD cells.

from the backplane. The distance between neighboring element centers is 0.75λ. Each dipole is made of two cylinders with square cross section of $1\Delta S' \times 1\Delta S'$, length of $9\Delta S'$, and feeding-gap size of $2\Delta S'$. The material of the whole BS antenna is set as copper with electric conductivity of $\sigma^{\mathrm{BS}} = 5.8 \times 10^7$ S/m.

With the trough reflector, the BS antenna radiates waves mainly in the $-x''$-direction. The required main lobe of the BS antenna can be formed by tuning amplitudes and phases excited in the four feeding-gaps of dipoles. In order to increase the effective distance of the BS antenna along the railway line, the declination angle of the main lobe is usually designed approximately $0.51°$ below the $x''o''y''$-plane (a horizontal plane) as illustrated in Fig. 1. For a linear dipole array with equal element spacing, it is usually exciting the dipoles with the

same amplitude but progressive phase shifts. The voltages between the feeding-gaps are represented by

$$U_l^{\text{elem}} = U_l^{\max} \sin\Big(2\pi f t + (l-1)\,\varphi^{\text{elem}}\Big), \quad l = 1, \ldots, 4 \tag{7}$$

where the voltage amplitude is set to $U_l^{\max} = 60.46\,\text{V}$, f is the excitation frequency, and φ^{elem} is the progressive phase shift. For the realization of the declination angle $\theta_{\text{dec}} = 0.51^\circ$, the progressive phase shift φ^{elem} is given by

$$\varphi^{\text{elem}} = \beta_0 d^{\,\text{elem}} \cos\big(\pi - \theta''_{\text{ml}}\big) \tag{8}$$

where β_0 is the wavenumber of free space, $d^{\,\text{elem}}$ is the element spacing, and $\theta''_{\text{ml}} = \theta_{\text{dec}} + \pi/2$ is the included angle between the $+z''$-direction and the main lobe direction. With these excitations, the normalized radiation pattern of BS antenna in $z''o''x''$-plane is obtained as shown in Fig. 6, where θ'' is the included angle between the $+z''$-axis and the vector $\mathbf{r}$ (from the center point o'' of the BS antenna to the far-field point), and ϕ'' is the included angle between the $+x''$-axis and the projection of $\mathbf{r}$ in $x''o''y''$-plane. On the closed sphere surface S_1 with radius of R_{S_1}, the θ''-polarized E-fields $E_\theta^{S_1}(R_{S_1}, \theta'', \phi'') = rE_\theta(r, \theta'', \phi'')/R_{S_1}$ are stored for subsequent predictions of wave propagation.

The FDTD method described above is used to implement the simulation of the terminal regions enclosed by S_1 and S_2. For the middle part of the entire RF downlink, the process of wave propagation from S_1 to S_2 will be simulated by the two-path propagation and multi-path statistical distribution models.

2.3. Combination With Two-Path Propagation Model

The two-path propagation model, which contains a direct wave and a reflected wave by the earth plane, is also called the deterministic analysis method, and is widely used in field-to-field prediction especially in a typical railway environment. In practice, the BS antenna is usually located at a long distance from locomotive antennas, such that the two-path waves can be traced from S_1 to S_2 using the method like ray-tracing. As depicted in Fig. 1, the direct ray and the reflected ray are generated from the center point o'' of the BS antenna and received at the center point o' of the locomotive antenna $1'$. The intersection points of the direct ray with S_1 and S_2 are denoted by p_{11} and p_{12} respectively, and the intersection points of the reflected ray with S_1, the earth plane and S_2 are denoted by p_{21}, p_{22} and p_{23} respectively. To the area enclosed by S_2, the two-path waves are considered as incident fields $\mathbf{E}_\theta^{\text{dir}}$ and $\mathbf{E}_\theta^{\text{ref}}$, and they are introduced

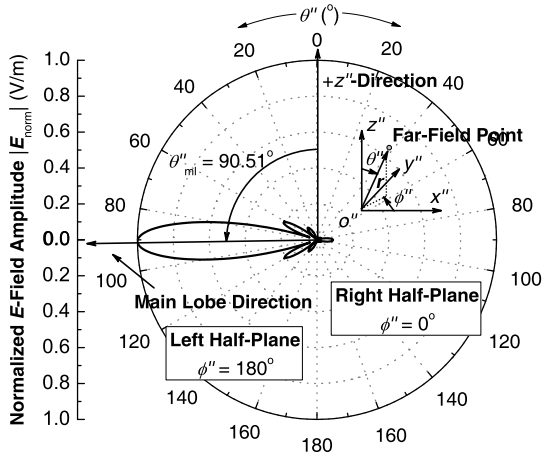

Figure 6. Normalized radiation pattern of BS antenna in $z''o''x''$-plane.

on the total-field/scattered-field connecting boundary (incorporating with S_2) of FDTD in the form of propagating plane waves

$$\begin{aligned}\mathbf{E}_{\theta}^{\mathrm{dir}}(\theta_d,\phi_d) &= R_{S_1}E_{\theta}^{S_1}\left(R_{S_1},\theta''_{\mathrm{dir}},\phi''_{\mathrm{dir}}\right)\frac{\mathrm{e}^{-\mathrm{j}\,\beta_0|\mathbf{r}_{\mathrm{dir}}|}}{|\mathbf{r}_{\mathrm{dir}}|}\hat{\boldsymbol{\theta}}_d\\ \mathbf{E}_{\theta}^{\mathrm{ref}}(\theta_r,\phi_r) &= R_{S_1}E_{\theta}^{S_1}\left(R_{S_1},\theta''_{\mathrm{ref}},\phi''_{\mathrm{ref}}\right)R_{\mathrm{TM}}\frac{\mathrm{e}^{-\mathrm{j}\,\beta_0|\mathbf{r}_{\mathrm{ref}}|}}{|\mathbf{r}_{\mathrm{ref}}|}\hat{\boldsymbol{\theta}}_r\end{aligned} \tag{9}$$

where the incident angles of the direct wave θ_d, ϕ_d, reflected wave θ_r, ϕ_r defined in o'-$x'y'z'$ coordinates, and the radiated angles of the direct wave θ''_{dir}, ϕ''_{dir}, reflected wave θ''_{ref}, ϕ''_{ref} defined in o''-$x''y''z''$ coordinates satisfy the following relations

$$\begin{aligned}&\theta_d = \pi - \theta''_{\mathrm{dir}}, \quad \phi_d = \phi''_{\mathrm{dir}} - \pi\\ &\theta_r = \theta''_{\mathrm{ref}}, \quad \phi_r = \phi''_{\mathrm{ref}} - \pi = \phi''_{\mathrm{dir}} - \pi = \phi_d.\end{aligned} \tag{10}$$

R_{S_1} in (9) is the radius of the sphere surface S_1, and is equal to $|o''p_{11}|$, $|o''p_{11}| = |o''p_{21}|$. The two-path vectors of direct and reflected waves are

$$\begin{aligned}\mathbf{r}_{\mathrm{dir}} &= \left(\left|o''o'\right| - \left|p_{12}o'\right|\right)\hat{\mathbf{r}}_{\mathrm{dir}} = \left|o''p_{12}\right|\hat{\mathbf{r}}_{\mathrm{dir}}\\ \mathbf{r}_{\mathrm{ref}} &= \left(\left|o''p_{22}\right| + \left|p_{22}o'\right| - \left|p_{23}o'\right|\right)\hat{\mathbf{r}}_{\mathrm{ref}} = \left(\left|o''p_{22}\right| + \left|p_{22}p_{23}\right|\right)\hat{\mathbf{r}}_{\mathrm{ref}}\end{aligned} \tag{11}$$

where $\hat{\mathbf{r}}_{\mathrm{dir}}$ and $\hat{\mathbf{r}}_{\mathrm{ref}}$ are unit vectors of the corresponding directions, and

$$\begin{aligned}\hat{\mathbf{r}}_{\mathrm{dir}} &= -\sin\theta_d\cos\phi_d\hat{\mathbf{x}} - \sin\theta_d\sin\phi_d\hat{\mathbf{y}} - \cos\theta_d\hat{\mathbf{z}}\\ \hat{\mathbf{r}}_{\mathrm{ref}} &= -\sin\theta_r\cos\phi_r\hat{\mathbf{x}} - \sin\theta_r\sin\phi_r\hat{\mathbf{y}} - \cos\theta_r\hat{\mathbf{z}}.\end{aligned} \tag{12}$$

R_{TM} in (9) is the Fresnel reflection coefficient of TM polarization wave, and is given by

$$R_{\mathrm{TM}} = \frac{\left(\varepsilon_r^{\mathrm{epl}} - \mathrm{j}60\lambda\sigma^{\mathrm{epl}}\right)\cos\vartheta - \sqrt{\left(\varepsilon_r^{\mathrm{epl}} - \mathrm{j}60\lambda\sigma^{\mathrm{epl}}\right) - \sin^2\vartheta}}{\left(\varepsilon_r^{\mathrm{epl}} - \mathrm{j}60\lambda\sigma^{\mathrm{epl}}\right)\cos\vartheta + \sqrt{\left(\varepsilon_r^{\mathrm{epl}} - \mathrm{j}60\lambda\sigma^{\mathrm{epl}}\right) - \sin^2\vartheta}} \tag{13}$$

where $\varepsilon_r^{\mathrm{epl}}$ and σ^{epl} are the relative permittivity and conductivity of the earth plane as listed in Table 1, ϑ is the incident angle to the earth plane, and $\vartheta = \pi - \theta''_{\mathrm{ref}} = \pi - \theta_r$.

2.4. Combination With Multi-path Statistical Distribution Model

As shown in Fig. 1, some obstacles may exist in the environment of the railway line and cause scattered waves. Therefore, the strength of the received signal at the locomotive terminal will oscillate randomly with the dynamic influence of the scattering from the environment. To achieve the goal of small-scale fading estimations, the statistical models for predicting the effect of the multi-path rays scattered from the random obstacles are necessary. In this paper, these scattered waves are introduced on S_2, and are given by

$$\mathbf{E}_m^{\mathrm{sca}}(\theta_m, \phi_m, \alpha_m) = E_m^0 \mathrm{e}^{\mathrm{j}\varphi_m}\hat{\boldsymbol{\gamma}}_m, \quad m = 1, 2, \ldots, n \tag{14}$$

where θ_m and ϕ_m are the incident angles as depicted in Fig. 1 (called zenithal angle and azimuthal angle respectively), α_m is the linear polarization angle rotating from θ_m-direction in $\theta_m\phi_m$-plane, E_m^0 and φ_m are the amplitude and phase angle, and the unit vector of direction is

$$\hat{\boldsymbol{\gamma}}_m = \cos\alpha_m\hat{\boldsymbol{\theta}}_m + \sin\alpha_m\hat{\boldsymbol{\phi}}_m. \tag{15}$$

Here, assume that θ_m, ϕ_m, α_m, E_m^0 and φ_m, or some of them vary randomly, and the variations obey the corresponding statistical distribution functions, as will be discussed in detail in Section 4. The center point o of S_2 is chosen as the reference phase center of the multi-path scattered waves numbered from 1 to n.

According to the above analyses, the incident fields arriving at the Rx antenna include the direct wave, ground-reflected wave and obstacle-scattered waves, and the complete field on S_2 is the superposition of them

$$\mathbf{E}_{S_2}^{\mathrm{inc}} = \mathbf{E}_\theta^{\mathrm{dir}} + \mathbf{E}_\theta^{\mathrm{ref}} + \sum_{m=1}^{n}\mathbf{E}_m^{\mathrm{sca}}. \tag{16}$$

Additionally, as depicted in Fig. 1 and Fig. 2, the surface S_2 is also intersected with other objects like the conducting wire, the steel rails and the earth plane, and $\mathbf{E}_{S_2}^{\text{inc}}$ should not be introduced on these intersection parts.

3. METHOD VERIFICATION

Figure 7 shows the receiving case of a quarter-wavelength monopole mounted upon a relatively large copper box at the top surface center. The rectangular box is a hollow structure with size of $2\,\text{m} \times 1\,\text{m} \times 1\,\text{m}$, thickness of one FDTD grid size, and electric conductivity of $\sigma = 5.8 \times 10^7\,\text{S/m}$. The illuminating field is set to be an uniform plane wave with operating frequency of 900 MHz and amplitude of $|\mathbf{E}_{\text{o}}^{\text{inc}}| = 1\,\text{V/m}$. Under this excitation scheme, the output voltage U_{out} and current I_{out} of the coax-fed monopole can be obtained by the method and settings in this paper. Fig. 8 exhibits the amplitude variations of U_{out} with different incident angles, and the results obtained by commercial software HFSS are also given in it for comparisons. As can be seen from the figure, the results are in well agreement with each other. The finite element mesh created by HFSS for the same coax-fed monopole is shown in Fig. 9. In HFSS simulation, the amplitude of the output voltage U_{out} is calculated by averaging the amplitude values of terminal voltage from U_1 to U_8, as illustrated in Fig. 9. A lumped port with impedance of $50\,\Omega$ is assigned at the end of the coaxial line. To achieve such an accuracy, the HFSS simulation for each point in Fig. 8 takes about 120 minutes on a PC with memory of 4 GB and CPU of 2.66 GHz, which is too much than that of the method of this paper.

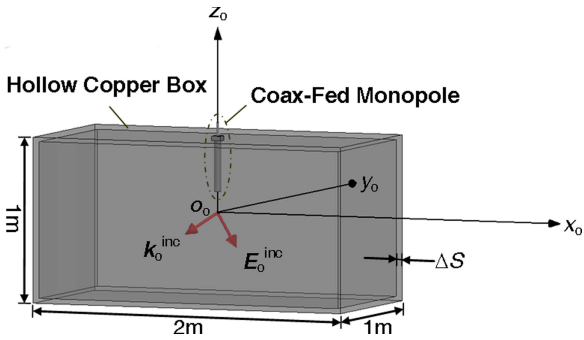

Figure 7. Verification model of quarter-wavelength monopole mounted on rectangular box top.

Figure 10 illustrates the current distribution on a straight wire scatterer with length of $h = 2\lambda$ and wire diameter of $2r_{\mathrm{o}} = \lambda/37.1$. The FDTD mesh size chosen here is $\lambda/36$. The operating frequency is 900 MHz. A plane wave with amplitude of $|\mathbf{E}_{\mathrm{o}}^{\mathrm{inc}}| = 1\,\mathrm{V}/(\lambda \sin\theta_{\mathrm{o}}^{\mathrm{inc}})$ is incident at angle of $\theta_{\mathrm{o}}^{\mathrm{inc}} = \pi/3$ in $\theta_{\mathrm{o}}^{\mathrm{inc}}$-polarization. The result from [25] obtained by the MoM for the same wire is also given for comparison. From Fig. 10, we can see that the result of this paper is in well agreement with that of [25].

The effectiveness of the infinity approximation used in this paper, has been verified in our previous work [26, 27].

4. NUMERICAL RESULTS AND DISCUSSION

The integrative modeling technique presented above was applied to study the small-scale fading characteristics of the RF downlink under the railway communication environment. As depicted in Fig. 1, the heights of the first locomotive antenna center o' and the BS antenna center o'' are set to $h_a = 3.87$ m and $h_b = 35$ m respectively. The length of the projection of line $o''o'$ in y-direction keeps at $|b_1b_2| = 30.83$ m while the train is moving in $+x$-direction, and at initial position of the train, the length of the projection of line $o''o'$ in x-direction is $|b_2o'| = 1000$ m.

The FDTD computation domain, where the locomotive antennas with the surrounding environment are modeled, is divided into $801 \times 131 \times 206$ cells, including 8 cells for PML modeling in the outer layer of the domain. The grid resolution is set to one tenth of the wavelength, so the space-step of FDTD is equal to $\Delta x = \Delta y = \Delta z = \Delta S = 0.0333$ m. To satisfy the Courant-Friedrichs-Lewy (CFL) stability condition, the FDTD time-step is chosen to $\Delta t = \Delta S/(2c) = 0.0556$ ns, where c is the velocity of light. The configuration parameters of the locomotive antennas are set to $a = 8$ mm, $b = 20.65$ mm and $\varepsilon_{rc} = 1.25$. Take the locomotive antenna $1'$ as the Rx antenna, the output voltage and current of the antenna would change with the incident fields introduced on S_2. After the precomputation test, the FDTD iteration number is set to 4000, which can give the stable results. When the position parameters of the BS antenna and the mobile locomotive antenna at each sampling point are given, the direct field and the ground-reflected field can be calculated by (9) and can be coupled into the FDTD computation domain through total-field/scattered-field connecting boundary.

According to the analysis of the high-speed railway wireless channel in [20], the direct and reflected waves (two-path) play a dominant role in signal transmission as manifested in [13, 14], while

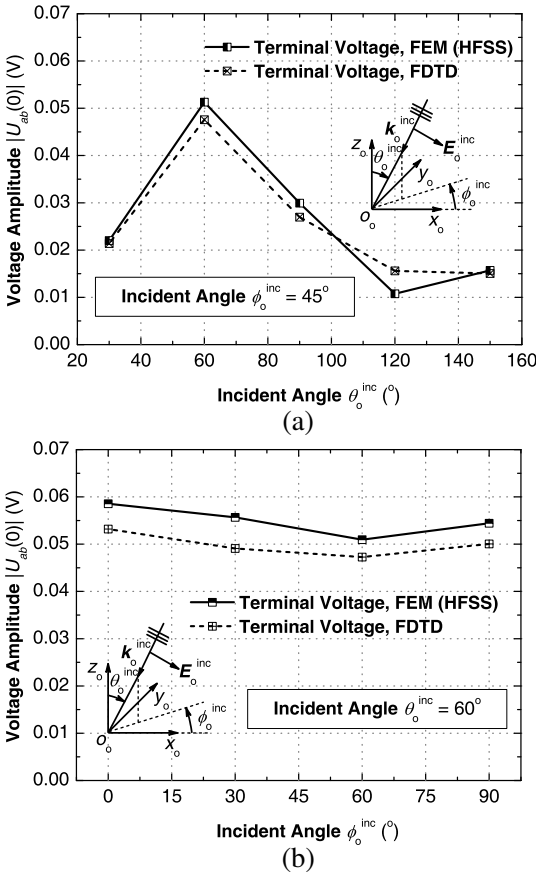

Figure 8. Variations of output voltage as function of incident angles. (a) θ_o^{inc}-direction, (b) ϕ_o^{inc}-direction.

the multi-path scattered waves are regarded as time-delayed and amplitude-attenuated signals as described in [21, 28]. Due to the multi-path effect, the scattered waves arriving at the antenna are sensitive with the location and with random phases. So the amplitude of complete field is dramatically varying with the moving of the train. A small changing of train (as small as a half-wavelength), will cause a large variation of receiving signal. This dramatic variation is defined as small-scale fading in [21]. In order to do the simulation for small-scale fading with high accuracy while the train is running at high-speed along the railway track, the interval of sampling points is set to 0.2λ, and totally twenty-one sampling points are considered. In the following

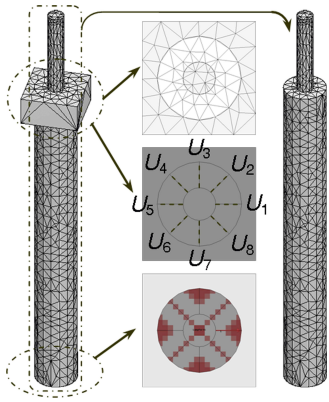

Figure 9. Finite element mesh and settings for coax-fed monopole model in HFSS.

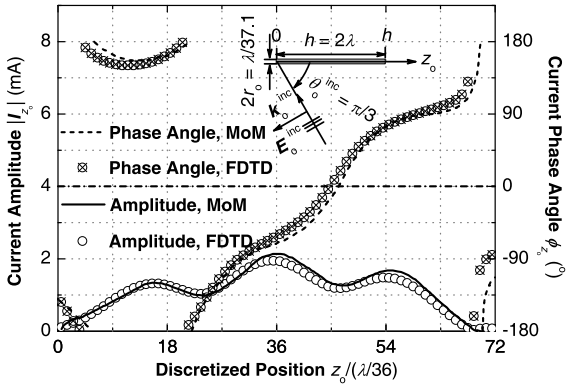

Figure 10. Current on wire scatterer.

analysis, three different statistical distribution models are used for the multi-path scattered fields prediction. These three models are derived based on [16, 29], and actually, they are acting as the second part of our entire RF link, as indicated in previous section. The corresponding numerical results under each situation are given in the subsequence.

4.1. Statistical Distribution Model I

We assume that there are total eight scattered fields illuminating on S_2 with various incident directions, amplitudes and phases. Here, for the first example, the scattered fields are assumed as spatial stationary waves with uniform amplitude of $E_m^0 = |\mathbf{E}_m^{\text{sca}}| = |\mathbf{E}_\theta^{\text{dir}}|/10^{0.8}$, $m =$

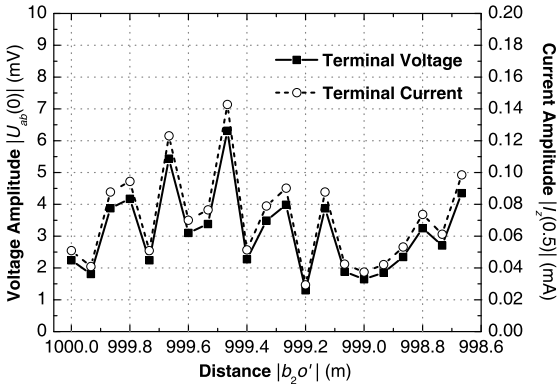

Figure 11. Variations of output voltage and current of locomotive antenna $1'$ with the location of sampling point, obtained by model I.

1, 2, ..., 8. The incident angles are $\theta_m = \pi/2$ and $\phi_m = m\pi/4$, and the polarization angle is $\alpha_m = 0$. Due to the moving of the train in $+x$-direction, the phase angles would be changed as

$$\varphi_m = \frac{m\pi}{4} + (i_s - 1)\,\beta_0 \Delta d_s \sin\theta_m \cos\phi_m, \quad m = 1, 2, \ldots, 8 \tag{17}$$

where i_s is the sampling point number from 1 to 21, and $\Delta d_s = 0.2\lambda$ is the sampling interval. The second term in (17) is caused by the path-difference at different sampling points. With the excitations of these eight scattered fields together with the direct and ground-reflected fields on S_2, the output voltage U_{out} and current I_{out} of the locomotive antenna $1'$ can be obtained after the iteration of FDTD. Fig. 11 shows the amplitude variations of U_{out} and I_{out} with the location of sampling point along the railway, where the output voltage has the same tendency as that of the output current, and the curves fluctuate very much within such a short-distance of about 1.33 m.

4.2. Statistical Distribution Model II

Different from the statistical distribution model I, second example considers the random variations of the incident directions and phases of the eight scattered fields when the train moving. Here, the random variable of the zenithal angle θ_m obeys the normal distribution (also called the Gaussian distribution) with the probability density function (PDF) of

$$P(\theta_m) = \frac{1}{\sqrt{2\pi}\tilde{\sigma}} \mathrm{e}^{-\frac{(\theta_m - \tilde{\mu})^2}{2\tilde{\sigma}^2}}, \quad 0 < \theta_m < \pi \tag{18}$$

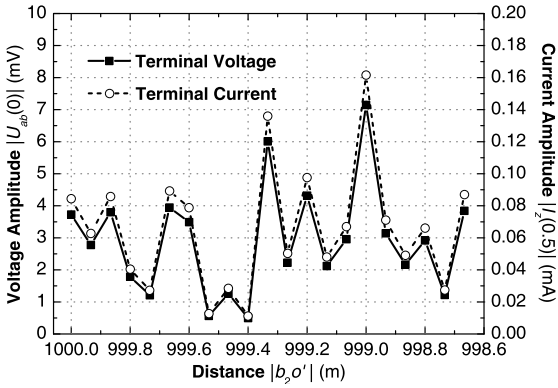

Figure 12. Variations of output voltage and current of locomotive antenna $1'$ with the location of sampling point, obtained by model II.

i.e., $\theta_m \sim \tilde{N}(\tilde{\mu}, \tilde{\sigma}^2)$ with mean of $\tilde{\mu} = 17\pi/36$ and variance of $\tilde{\sigma}^2 = (9/\pi)^2$. The random variables of the azimuthal angle ϕ_m and the phase angle φ_m obey the uniform distribution with the PDFs of

$$P(\phi_m) = \frac{1}{2\pi}, \quad 0 < \phi_m < 2\pi$$
$$P(\varphi_m) = \frac{1}{2\pi}, \quad 0 \le \varphi_m \le 2\pi \tag{19}$$

i.e., $\phi_m \sim \tilde{U}(0, 2\pi)$ and $\varphi_m \sim \tilde{U}(0, 2\pi)$. At the sampling points numbered from 1 to 21, the values of θ_m, ϕ_m and φ_m ($m = 1, 2, \ldots, 8$) are chosen from the corresponding sample spaces. They are actually the pseudo-random numbers generated by setting the states of corresponding random number generators from 1 to 21, from 1 to 21 and from 1001 to 1021 respectively. The other parameters of the scattered fields are set as the same as in statistical distribution model I. Fig. 12 shows the different amplitude variations of U_{out} and I_{out} on the locomotive antenna $1'$, where the fluctuation of curves is also very significant.

4.3. Statistical Distribution Model III

Based on the statistical distributions for the incident angles θ_m and ϕ_m used in the second example, the model III here contains more random parameters for the amplitude E_m^0, phase angle φ_m and polarization angle α_m of the scattered fields. The amplitude E_m^0 in (14) is rewritten

by

$$E_m^0 = |\mathbf{E}_m^{\text{sca}}| = \frac{\left|\mathbf{E}_\theta^{\text{dir}}\right|}{10^{0.8}} \left|R_{\text{TE}}^m\right|. \tag{20}$$

The relative attenuation R_{TE}^m in (20), which indicates the scattering capability of different obstacles composed of random mediums, is represented by the Fresnel reflection coefficient of TE polarization wave

$$R_{\text{TE}}^m = \frac{\cos\vartheta_s^m - \sqrt{(\varepsilon_r^m - j60\lambda\sigma^m) - \sin^2\vartheta_s^m}}{\cos\vartheta_s^m + \sqrt{(\varepsilon_r^m - j60\lambda\sigma^m) - \sin^2\vartheta_s^m}} \tag{21}$$

where ϑ_s^m, ε_r^m and σ^m are the reflected angle, relative permittivity and electric conductivity of the random medium respectively. Here, the random variables of ϑ_s^m, ε_r^m and σ^m obey the uniform distribution of $\vartheta_s^m \sim \tilde{U}(0, \pi/2)$, the normal distribution of $\varepsilon_r^m \sim \tilde{N}(15, 4^2)$ and the normal distribution of $\sigma^m \sim \tilde{N}(0.005, 0.0015^2)$ respectively with the states of corresponding random number generators all set from 1 to 21. The phase composed of a component caused by differential time-delay τ_m^{dif}(s) and an additional phase shift φ_m^{add} is given by

$$\varphi_m = -2\pi f \left(10^{-6}\tau_m^{\text{dif}}\right) - \varphi_m^{\text{add}} \tag{22}$$

where φ_m^{add} is chosen as the same as the former φ_m in (19) of the second example. The random variable of τ_m^{dif} (μs) in (22) obeys the exponential distribution with the PDF of

$$P\left(\tau_m^{\text{dif}}\right) = \tilde{\lambda}\mathrm{e}^{-\tilde{\lambda}\tau_m^{\text{dif}}}, \quad \tau_m^{\text{dif}} > 0 \tag{23}$$

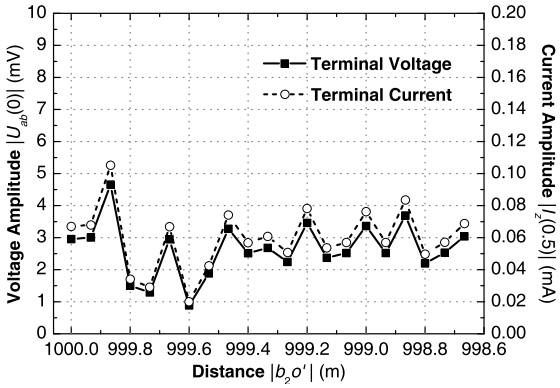

Figure 13. Variations of output voltage and current of locomotive antenna $1'$ with the location of sampling point, obtained by model III.

i.e., $\tau_m^{\text{dif}} \sim \tilde{E}(\tilde{\lambda})$ with $\tilde{\lambda} = 0.47$, and the state of the random number generator is set from 1 to 21. Also, the polarization direction would change by effects of anisotropic medium. The random variable of α_m is assumed to obey the uniform distribution of $\alpha_m \sim \tilde{U}(0, 2\pi)$ with the state of the random number generator set from 2001 to 2021. Under these new settings for the scattered fields, the variations of the output voltage and current of the locomotive antenna $1'$ is depicted in Fig. 13. By comparison of Fig. 13 with Fig. 11 and Fig. 12, we can find that the average variations of the curves are in the same order of magnitude, and $|U_{\text{out}}|$ and $|I_{\text{out}}|$ have the same tendency when the terminal impedance is $50\,\Omega$. However, due to the effects of multi-path scattered waves, three dissimilar fluctuation characteristics can be observed.

5. CONCLUSION

Estimation for the small-scale fading characteristics of the RF wireless link is an important work especially for the complicated communication environment of high-speed railway. An integrative modeling technique involving the full-wave numerical method, ray-tracing method and statistical method is proposed here. The procedure of the integrative modeling technique starts from the input terminal of the BS antenna and ends up with the output terminal of the train antenna mounted on the locomotive top. Compared to the conventional methods, which can be used to estimate the radio wave propagation characteristics by field-to-field prediction in relatively open environments, the proposed method in this paper can take into account the interactions between the antennas and the complicated surrounding environments. A two-path propagation model and three multi-path statistical distribution models are integrated into the approach respectively, which connects the link terminals (Tx/Rx antennas with their neighboring areas) and the open space. From the results of the RF downlink obtained in this paper, we can conclude that the significant small-scale fluctuations will occur if there are random scattered waves coming from different directions. Thereby, in order to see the fluctuation clearly, high sampling rate and adequate sampling points are needed. This can be done efficiently by the proposed integrative modeling technique.

ACKNOWLEDGMENT

This work was supported in part by the National Natural Science Foundation of China under Grant No. 60825101, and in part by the National High-Tech. Research & Development Program (863 Program) of China under Grant 2008AA01Z224. Also, the authors would like to

thank all the editors and reviewers for their very helpful suggestions and comments for improving this paper.

REFERENCES

1. Pu, S. and J.-H. Wang, "Research on the receiving and radiating characteristics of antennas on high-speed train using integrative modeling technique," *Proc. 11th Asia Pacific Microwave Conference*, 1072–1075, 2009.
2. Iskander, M. F. and Z. Yun, "Propagation prediction models for wireless communication systems," *IEEE Trans. Microwave Theory Tech.*, Vol. 50, No. 3, 662–673, 2002.
3. Sarkar, T. K., Z. Ji, K. Kim, A. Medouri, and M. Salazar-Palma, "A survey of various propagation models for mobile communication," *IEEE Antennas Propag. Mag.*, Vol. 45, No. 3, 51–82, 2003.
4. Kara, A. and E. Yazgan, "Modelling of shadowing loss due to huge non-polygonal structures in urban radio propagation," *Progress In Electromagnetics Research B*, Vol. 6, 123–134, 2008.
5. Okumura, Y., E. Ohmori, T. Kawano, and K. Fukuda, "Field strength variability in VHF and UHF land mobile service," *Rev. Elect. Comm. Lab.*, Vol. 16, No. 9–10, 825–873, 1968.
6. Landstorfer, F. M., "Wave propagation models for the planning of mobile communication networks," *Proc. 29th European Microwave Conference*, 1–6, 1999.
7. El-Sallabi, H. M. and P. Vainikainen, "Radio wave propagation in perpendicular streets of urban street grid for microcellular communications. Part I: Channel modeling," *Progress In Electromagnetics Research*, Vol. 40, 229–254, 2003.
8. Giampaolo, E. Di and F. Bardati, "A projective approach to electromagnetic propagation in complex environments," *Progress In Electromagnetics Research B*, Vol. 13, 357–383, 2009.
9. Meng, Y. S., Y. H. Lee, and B. C. Ng, "Study of propagation loss prediction in forest environment," *Progress In Electromagnetics Research B*, Vol. 17, 117–133, 2009.
10. Ikegami, F., S. Yoshida, T. Takeuchi, and M. Umehira, "Propagation factors controlling mean field strength on urban streets," *IEEE Trans. Antennas Propag.*, Vol. 32, No. 8, 822–829, 1984.
11. Hoppe, R., P. Wertz, F. M. Landstorfer, and G. Wölfle, "Advanced ray-optical wave propagation modelling for urban and

indoor scenarios including wideband properties," *Euro. Trans. Telecomms.*, Vol. 14, No. 1, 61–69, 2003.

12. Paran, K. and N. Noori, "Tuning of the propagation model itu-R P.1546 recommendation," *Progress In Electromagnetics Research B*, Vol. 8, 243–255, 2008.
13. Hattori, T., K. Abe, and K. Abe, "Analyses of propagation characteristics in future railway communication systems using 25 GHz band radio," *Proc. 49th IEEE Veh. Tech. Conf.*, 2288–2292, 1999.
14. Nakamura, K., K. Kawasaki, and M. Shindo, "Development of methods for the calculation of radio propagation characteristics in the railway environment," *Quarterly Report of Railway Technical Research Institute*, Vol. 43, No. 4, 182–186, 2002.
15. Chen, Y., Z. Zhang, L. Hu, and P. B. Rapajic, "Geometrybased statistical model for radio propagation in rectangular office buildings," *Progress In Electromagnetics Research B*, Vol. 17, 187–212, 2009.
16. Taga, T., "Analysis for mean effective gain of mobile antennas in land mobile radio environments," *IEEE Trans. Veh. Tech.*, Vol. 39, No. 2, 117–131, 1990.
17. Chen, Y., Z. Zhang, and T. Qin, "Geometrically based channel model for indoor radio propagation with directional antennas," *Progress In Electromagnetics Research B*, Vol. 20, 109–124, 2010.
18. Chou, H.-T. and H.-T. Hsu, "Hybridization of simulation codes based on numerical high and low frequency techniques for the efficient antenna design in the presence of electrically large and complex structures," *Progress In Electromagnetics Research*, Vol. 78, 173–187, 2008.
19. Hsu, H.-T., F.-Y. Kuo, and H.-T. Chou, "Convergence study of current sampling profiles for antenna design in the presence of electrically large and complex platforms using FIT-UTD hybridization approach," *Progress In Electromagnetics Research*, Vol. 99, 195–209, 2009.
20. Pu, S., J.-H. Wang, and Z. Li, "Integrative modeling and analyses of the wireless link for communication system in railway environment," *Proc. 8th International Symposium on Antennas, Propagation and EM Theory*, 1322–1325, 2008.
21. Sklar, B., "Rayleigh fading channels in mobile digital communication systems. Part I: Characterization," *IEEE Commun. Mag.*, Vol. 35, No. 9, 136–146, 1997.
22. Yee, K. S., "Numerical solution of initial boundary value problems

involving Maxwell's equations in isotropic media," *IEEE Trans. Antennas Propag.*, Vol. 14, No. 3, 302–307, 1966.

23. Gedney, S. D., "An anisotropic perfectly matched layer-absorbing medium for the truncation of FDTD lattices," *IEEE Trans. Antennas Propag.*, Vol. 44, No. 12, 1630–1639, 1996.
24. Maloney, J. G., K. L. Shlager, and G. S. Smith, "A simple FDTD model for transient excitation of antennas by transmission lines," *IEEE Trans. Antennas Propag.*, Vol. 42, No. 2, 289–292, 1994.
25. Harrington, R. F., *Field Computation by Moment Methods*, Macmillan, New York, 1968.
26. Wang, J.-H. and H. Zhang, "Velocity compensated coplanar wave guide bend for odd-mode suppression," *Microwave Opt. Technol. Lett.*, Vol. 50, No. 5, 1201–1204, 2008.
27. Zhang, H., J.-H. Wang, and W.-Y. Liang, "Study on the applicability of extracted distributed circuit parameters of non-uniform transmission lines by equivalent circuit method," *Journal of Electromagnetic Waves and Applications*, Vol. 22, No. 5–6, 839–848, 2008.
28. Yarkony, N. and N. Blaunstein, "Prediction of propagation characteristics in indoor radio communication environments," *Progress In Electromagnetics Research*, Vol. 59, 151–174, 2006.
29. Clarke, R. H., "A statistical theory of mobile-radio reception," *Bell Syst. Tech. J.*, Vol. 47, No. 6, 957–1000, 1968.